IEEE Photonics Journal
An IEEE Photonics Society Publication

Open Access

Non-Destructive Three-Dimensional Optical Imaging of a Fiber Bragg Grating

Volume 6, Number 5, October 2014

Xiao Ming Goh
Shan Shan Kou
Betty P. Kouskousis
Nicoleta M. Dragomir
Stephen F. Collins
Greg W. Baxter
Ann Roberts

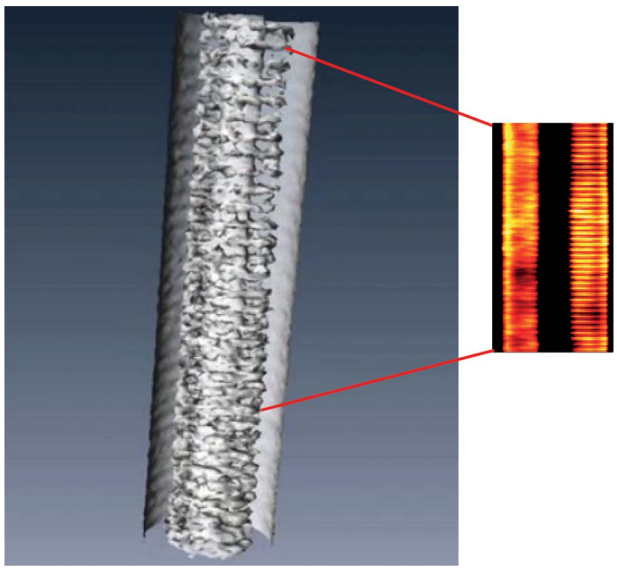

DOI: 10.1109/JPHOT.2014.2360282
1943-0655

IEEE photonics SOCIETY

IEEE

Non-Destructive Three-Dimensional Optical Imaging of a Fiber Bragg Grating

Xiao Ming Goh,[1,2] Shan Shan Kou,[1] Betty P. Kouskousis,[3] Nicoleta M. Dragomir,[1] Stephen F. Collins,[3] Greg W. Baxter,[3] and Ann Roberts[1]

[1]School of Physics, The University of Melbourne, Melbourne, VIC 3010, Australia
[2]Now at Institute of Materials Research and Engineering, A*STAR, Singapore 117602
[3]Optical Technology Research Laboratory, College of Engineering and Science, Victoria University, Melbourne, VIC 8001, Australia

DOI: 10.1109/JPHOT.2014.2360282

Manuscript received August 11, 2014; revised September 3, 2014; accepted September 4, 2014. Date of publication September 25, 2014; date of current version October 9, 2014. This work was supported in part by the Australian Research Council under the Discovery Projects Scheme DP0878346. The work of S. S. Koh was supported by the Australian Research Council under through ARC DECRA Fellowship under Project DE 120102352. Media 1 gives the 3-D rendered video of the reconstructed core of the FBG. Note that in the video, the core and cladding of the FBG have been made transparent so as to show only the reconstructed grating structures. The file size is 981 KB. The file is best viewed with Windows Media Player, Version 12.0.7601.18150. Corresponding author: A. Roberts (e-mail: ann.roberts@unimelb.edu.au).

Abstract: Here, we demonstrate a non-destructive quantitative phase imaging method, in conjunction with tomographic reconstruction techniques, to reconstruct the three-dimensional refractive index distribution of a fiber Bragg grating. In addition to being able to extract the fundamental period of the grating, we are able to reconstruct the refractive index profile of the fiber core and index variations associated with the grating.

Index Terms: Fiber gratings, three-dimensional microscopy, optical properties of photonic materials.

1. Introduction

Fiber Bragg Gratings (FBGs) serve as versatile components in a wide range of applications, particularly in the areas of sensing and telecommunications [1]. A FBG possesses a characteristic periodic variation in refractive index (RI) along the length of the fiber core, typically formed by exposing a section of the photosensitive optical fibre to ultraviolet (UV) light [2], [3] that has been transmitted through a phase mask. Diffraction produced by the mask creates an interference pattern within the fiber, inducing a periodic variation in the RI along its length. Ideally, a phase mask with a period of Λ_{pm} diffracts light into only the ± 1 diffracted orders to form a set of fringes perpendicular to the direction of the UV beam with a period of $\Lambda_{pm}/2$ [1]. Imperfect suppression of the zeroth and higher diffraction orders from the mask, however, leads to the formation of a complex pattern of interleaved fringes with a period of Λ_{pm} behind the mask [4]. This results in phase-mask-written FBGs exhibiting a 3-D periodic RI structure that is more complex than would be anticipated in the case of only two diffracted orders. This complex 3-D structure can be attributed to the Talbot diffraction pattern produced by the interference of multiple diffracted orders and which replicates the periodic grating pattern at a distance from the phase mask characterized by the Talbot length [5].

The resulting complex structure of the FBGs was initially observed using various forms of microscopy [4]–[9]. These reports were followed by theoretical analysis of grating formation [4], [10] and the identification of features in the transmission spectrum in the FBGs attributable to artifacts arising from the use of a phase mask in fabrication [11]. In particular, the dual periodicities (Λ_{pm} and $\Lambda_{pm}/2$) exhibited by FBGs written with the phase mask technique have been observed by use of Differential Interference Contrast (DIC) microscopy [6], and compared with simulated DIC images [7] predicted by the interference pattern formed from the phase mask used in [6]. Given the complex periodic structure exhibited by FBGs, however, it is clearly of interest to obtain full 3-D information about the variation of the RI distribution within the fiber core. Furthermore, as details of the FBG structure within the fiber core affect the spectral performance of the FBG [12], a full 3-D reconstruction of the fiber core serves to illuminate issues pertaining to these intriguing effects.

Here, we demonstrate the use of a non-destructive, quantitative, 3-D optical imaging technique for examining a section of the core of a FBG inscribed in the core of an optical fiber. Quantitative phase microscopy (QPM) [13] is a non-interferometric, non-destructive imaging technique that can be used with partially coherent light in a conventional bright-field microscope for determining the phase shift introduced into an optical wavefield by a transparent specimen. One advantage of QPM over its counterparts is the ability to provide simultaneous, but separate, quantitative information about both the absorption by the specimen and the phase [14]. This technique has been demonstrated in conjunction with standard tomographic techniques for reconstructing the 3-D RI distribution of axially symmetrical optical fibers [15], and fibers exhibiting a variation in RI along the length [16], [17] including long period gratings [17]. In this paper, we extend the preliminary results presented in a conference paper [18] and extract detailed quantitative 3-D RI information about the core of the fiber and the FBG obtained using Quantitative Phase Tomography (QPT). It should be noted that the sensitivity and spatial resolution required is significantly more challenging than imaging long period gratings. For example, long period gratings may have grating periods of the order of a millimeter, with index variation of the order of 1×10^{-3} [17]. In contrast, FBGs may have periods of the order of microns. Moreover, given the weak phase variation typical in FBGs [11] and the small period of its structure, the 3-D imaging of the FBG serves to demonstrate the capability of the technique in reconstructing small RI variations such as those exhibited by FBGs.

2. Methods and Materials

The FBG investigated here was inscribed at a wavelength of 244 nm and a CW power of 222 mW with a 4-min exposure using a phase mask (Lasiris with a period of 1.057 ± 0.0005 μm positioned over a single-mode fibre (Corning SMF-28, 125.0 ± 0.7 μm cladding diameter, 8.2 ± 0.4 μm core diameter) that had been preloaded with H_2. Taking into account the distribution of power into the various diffracted orders produced by the phase grating [6], [7], computed intensity distribution within the fiber, assuming a medium refractive index of 1.469, are shown in Fig. 1 along with a schematic showing the coordinate system used. In these calculations, the values of [7] are used: 0.09% power into the zeroth order, 39.5% and 36.7% into the ± 1 diffracted orders and 3.9% and 4.6% into the ± 2 orders [19]. The period, Λ_{pm}, is assumed to be 1.057 μm giving a Talbot length of 13.42 μm. The influence of the source coherence was not included in the calculations as were variations in transmission across the fiber boundary. The phase mask was assumed to be illuminated from the *x*-direction. Complete data is provided in Reference [7]. It should be noted that the medium of refractive index employed here is the value for silica glass at the UV regime, i.e., higher than the more widely known value (1.444) at near-infrared wavelengths where the fiber was employed.

Profiles along the z-direction obtained through Fig. 1(a) separated by 6.71 μm (half the Talbot length) are shown in Fig. 1(c). The existence of fringes at the dominant period Λ_{pm} and a weaker periodicity at the design period $\Lambda_{pm}/2$ are also apparent in Fig. 1(a). A 180° phase shift in the fringe pattern in the xz plane across the fiber (in the x-direction) is also evident over the half the Talbot length as expected.

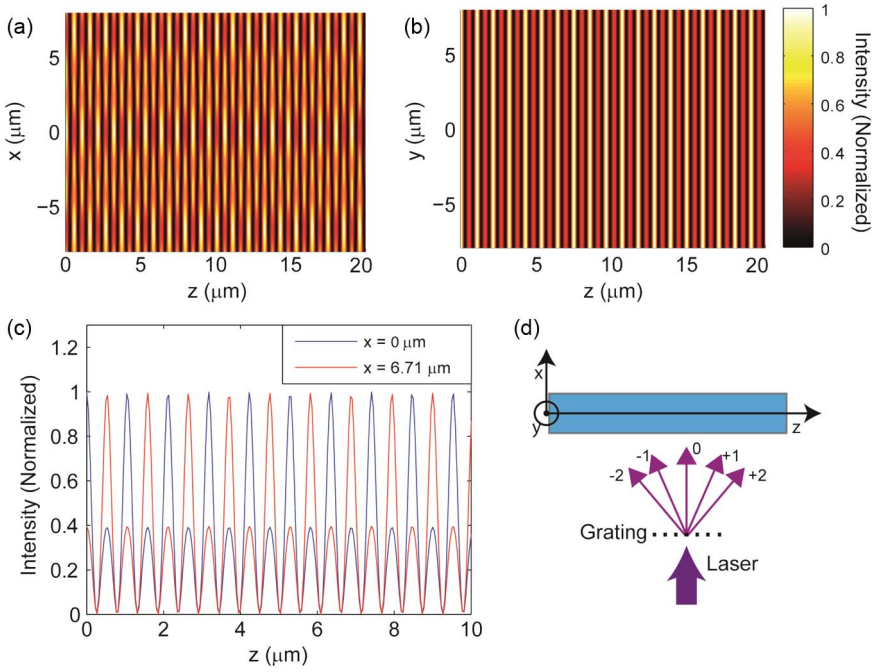

Fig. 1. Simulated intensity distributions behind the phase grating with 0, ±1, and ±2 diffracted orders of intensity given in the text. Surface plots show the intensity behind the grating in the (a) *xz*-plane and (b) *yz*-plane, while (c) shows profiles through the *x*–*z* plane along two lines separated by half the Talbot length. A schematic defining the coordinates used is given in (d).

In-focus and out-of-focus $(\pm 1.2\ \mu\text{m})$ intensity images of the sample were obtained using a $40\times$ objective (Olympus UplanApo $40\ \times$ 0.85 N.A.) on a conventional bright-field transmission microscope (Olympus BX60) equipped with a CCD camera (Roper Scientific Cool-SNAP HQ) at 521 nm. The fiber was immersed in a pool of index matching fluid $(\text{n} = 1.4580 \pm 0.0002)$ (Cargille Laboratories) formed between two other identical fibers located on each side of the specimen. A custom tomographic mount provided control of the rotation of the fiber sample about its longitudinal axis within the confines of the optical microscope area. Further details of equipment specifications and the image acquisition procedure can be found in our previous work [16].

A transverse phase measurement through the fiber represents a single projection through the fiber RI distribution under weak object conditions. The 3-D RI reconstruction of the fiber can be determined by applying tomographic reconstruction techniques based on the projection-slice theorem to a series of 2-D phase measurements, which were obtained through a 180° rotation. In order to apply the projection-slice theorem for reconstructing the 3-D RI distribution within the FBG, quantitative phase measurements were obtained for each angular position by use of QPM [13]. Here, a total of 180 transverse phase images of the fiber were obtained at angular intervals of 1°. Three bright field intensity images at a defocus distance of 1.2 μm were used to recover one phase measurement for each angular position. Fig. 2 shows examples of transverse bright field intensity images of a section $(50\ \mu\text{m} \times 42.5\ \mu\text{m})$ of the FBG core at angular orientations of the fiber separated by 45°. In Fig. 2(a), the core exhibits a uniformly parallel grating structure that is clearly seen throughout the fibre core and which corresponds to the set of fringes perpendicular to the direction of the writing UV laser beam. Here, we define the rotation angle of the fiber to be $\theta = 0$ for this particular orientation of the gratings. As the fiber is rotated about its longitudinal axis, the grating structure exhibits a gradual change as observed from Fig. 2(b) and (c). In particular, at 90° from the position of the fiber shown in Fig. 2(a), the intensity distribution of the grating structure appears as interleaved sets of fringes as is also the case in Fig. 2(c). The grating structures here are less perceptible within the central region of the fiber core, instead, exhibiting greater distinction at the edges of the core. This is a

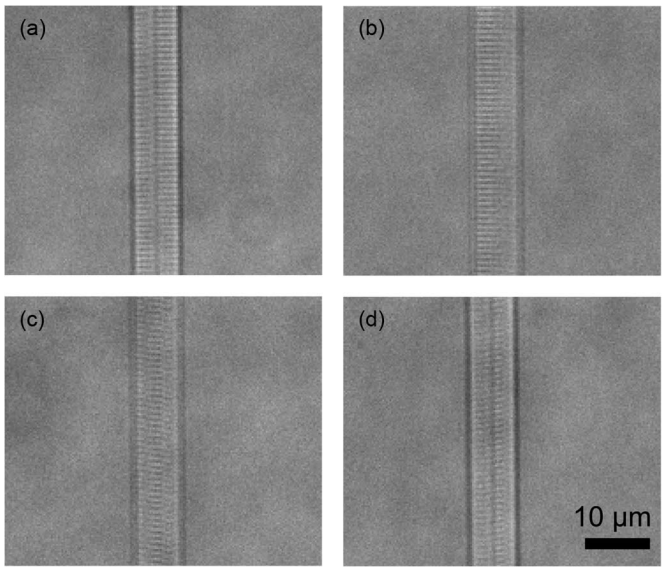

Fig. 2. Transverse bright field images of a section of the FBG at angular rotation angles (a) $\theta = 0°$, (b) $\theta = 45°$, (c) $\theta = 90°$, and (d) $\theta = 135°$ taken at 1.2 μm negative defocus. Each section of the fibre shown is 50 μm $\times$ 42.5 μm.

consequence of the dip in the center of the core refractive index profile; an artifact of the fiber fabrication technique.

Given that the mechanical parts of the tomographic mount introduced shifts both laterally and longitudinally as the fiber was rotated, accurate alignment of the phase images was important prior to processing the 2-D phase maps with the tomographic algorithms. Each series of phase images was aligned in the lateral direction using an edge detection algorithm. The RI distribution of a series of transverse slices through the fiber was calculated from aligned phase images using filtered backprojection [20], [21], achieved by applying the inverse Radon Transform [22] to the phase data with a ramp filter [23]. Here, the standard inverse Radon transformation in IDL version 8.1.0 Research Systems, Inc. was applied.

3. Results and Discussion

The reconstructed 3-D RI distribution of the FBG is shown in Fig. 3. The structure of the core of the fiber, with a diameter of approximately 10 μm, is apparent. The difference in RI between the core and the cladding is $\sim 4.5 \times 10^{-3}$ with a distinct dip in the center of the core. These results are consistent with those published previously [6]. The core of the reconstructed fiber is plotted along the x or y-axes. Fourier transformation of Fig. 3(a) gives a spatial frequency for the grating of 5.79 $\pm$ 0.03 rad/μm giving a periodicity of 1.085 $\pm$ 0.005 μm and the variation in index is $\sim 2 \times 10^{-4}$. The slight discrepancy between the periodicity determined here and that found independently [6] ($\sim$2%) is likely due to a slight miscalibration of the microscope. It can be observed that the reconstructed 3-D periodic grating structures shown in Fig. 3(a) and (b) are not identical. This observation is anticipated given the presence of the two distinct grating structures that can be perceived upon a 90° rotation of the fiber as discussed earlier.

Clearly, the reconstructed core in Fig. 3(a) exhibits uniformly parallel grating structures, thus corresponding to the set of fringes formed in the direction parallel to the writing UV laser beam. Fig. 3(b) shows the interleaved sets of grating structure characteristic of this particular FBG upon a 90° rotation, reflecting the influence of the Talbot diffraction pattern. In contrast to the periodic grating which can clearly be discerned in Fig. 3(a), the interleaved grating structure of Fig. 3(b) exhibits weaker contrast. Profiles through the RI distribution in the xz- and yz-planes are shown in Fig. 4. The two profiles are separated by a distance equal to approximately half

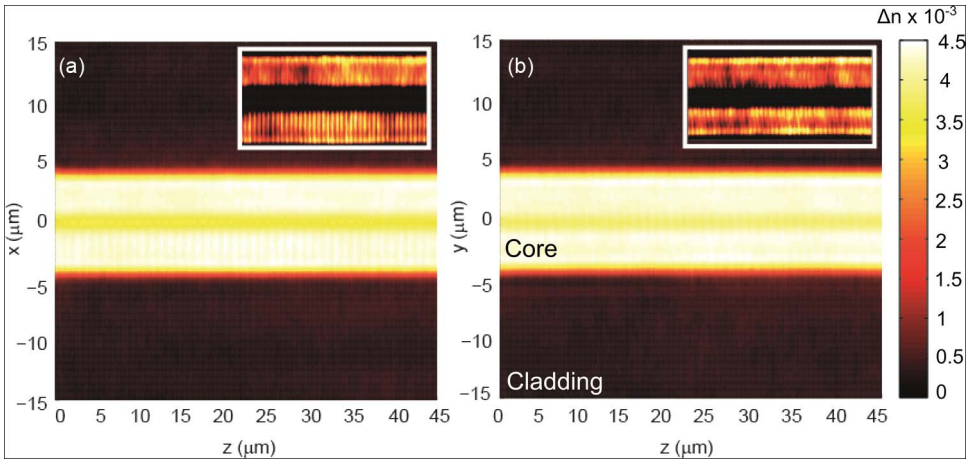

Fig. 3. False colored tomographic reconstruction of a section the FBG. 3-D volume rendering of the RI distribution of the fiber sectioned along the (a) x and (b) y-axis with the cladding rendered transparent to show the bisected fiber. (Inset) Reconstructed RI distribution of the bisected core with a modified colormap showing the (a) *xz*- and (b) *yz*-planes.

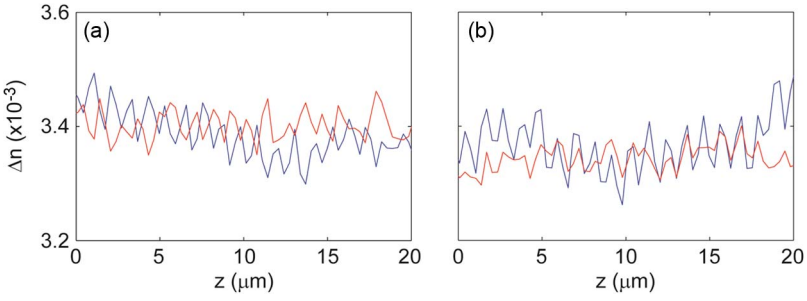

Fig. 4. Profiles (blue and red lines) parallel to the z-axis through the data of Fig. 3 separated by a distance of 6.77 μm (close to half the Talbot length of 6.71 μm). These show the (a) presence or (b) absence of a phase shift between the two profiles in the (a) *x*–*z* plane and (b) *y*–*z* planes.

the computed Talbot length. In the case of the profile through the xz-plane (see Fig. 4(a)), this suggests that the grating structures should be 180° out of phase. Despite the noise in the recovered profiles, these profiles provide evidence that this is the case. Furthermore, we would not expect this phase shift to be present in the corresponding profiles through the yz-plane (see Fig. 4(b)), which is again supported by the data.

In addition, it is interesting to note that the reconstructed 3-D RI mapping shows an asymmetry across the z-axis for sections through both the xz- (see Fig. 3(a)) and yz-planes (see Fig. 3(b)) of the fiber core. In the magnified reconstructed fiber cores shown as insets in Fig. 3, it is apparent that the reconstructed gratings typically exhibit a stronger contrast in one quadrant of the fiber core. This asymmetry in contrast is particularly noticeable in Fig. 3(a) where the grating structures in the lower quadrant of the reconstruction are clearly more distinct in comparison to those in the top half of the quadrant. This observation persists in the reconstructed grating structures and holds true throughout various rotation angles of the fiber as shown in the 3-D rendered video of the reconstructed core (Media 1). This asymmetry could be due to absorption in the fiber core reducing the intensity of the writing field in the core. The first frame of the video of the reconstructed fiber core as it is rotated about its longitudinal axis is shown in Fig. 5. Note that in the video, the core and cladding of the FBG have been made transparent so as to show only the reconstructed grating structures. Here, the 3-D video rendering was performed using the 3-D visualization software, Amira, VSG [24].

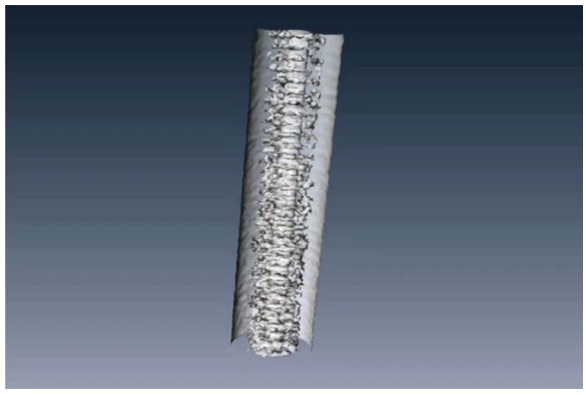

Fig. 5. Single-frame excerpt from the 3-D rendering of the reconstructed fiber core (Media 1).

The two interchanging grating structures characteristic of this particular FBG upon a 90° rotation can also be clearly observed in the 3-D rendered video. In agreement with previous observations [25], this effect may be attributed to the grating inscription process, where the area of the fiber closer to the laser exhibits a higher resultant RI than the area further away given that the writing beam is attenuated on propagation by the photosensitive core of the fiber.

4. Conclusion

In conclusion, we have demonstrated the 3-D RI reconstruction of a FBG using a non-destructive tomographic technique. Application of QPT has enabled the complex 3-D RI distribution within the FBG core, comprising periodic gratings structures to be clearly discerned, revealing a difference in RI between the core and the cladding to be $\sim 4.5 \times 10^{-3}$. In particular, the two distinct grating structures characteristic of this particular FBG as a result of the phase-mask writing process was clearly discerned in the 3-D RI reconstructions. Furthermore, QPT has facilitated the observation of an asymmetry in the reconstructed RI distribution where the gratings exhibited clearer contrast in certain sections of the fiber core—a feature that is consistent with previous observations. Given its non-destructive nature, this technique is also advantageous for application to the imaging of biological samples.

References

[1] R. Kashyap, *Fiber Bragg Gratings*. San Diego, CA, USA: Academic, 1999.
[2] K. O. Hill, B. Malo, F. Bilodeau, D. C. Johnson, and J. Albert, "Bragg gratings fabricated in monomode photosensitive optical fiber by UV exposure through a phase mask," *Appl. Phys. Lett.*, vol. 62, no. 10, pp. 1035–1037, Mar. 1993.
[3] G. Meltz, W. W. Morey, and W. H. Glenn, "Formation of Bragg gratings in optical fibers by a transverse holographic method," *Opt. Lett.*, vol. 14, no. 15, pp. 823–825, Aug. 1989.
[4] P. E. Dyer, R. J. Farley, and R. Giedl, "Analysis of grating formation with excimer laser irradiated phase masks," *Opt. Commun.*, vol. 115, no. 3–4, pp. 327–334, Mar. 1995.
[5] J. D. Mills, C. W. Hillman, B. H. Blott, and W. S. Brocklesby, "Imaging of free-space interference patterns used to manufacture fiber Bragg gratings," *Appl. Opt.*, vol. 39, no. 33, pp. 6128–6135, Nov. 2000.
[6] N. M. Dragomir *et al.*, "Nondestructive imaging of a type I optical fiber Bragg grating," *Opt. Lett.*, vol. 28, no. 10, pp. 789–791, May 2003.
[7] B. P. Kouskousis *et al.*, "Quantitative investigation of the refractive-index modulation within the core of a fiber Bragg grating," *Opt. Express*, vol. 14, no. 22, pp. 10 332–10 338, Oct. 2006.
[8] C. W. Smelser *et al.*, "Multiple-beam interference patterns in optical fiber generated with ultrafast pulses and a phase mask," *Opt. Lett.*, vol. 29, no. 13, pp. 1458–1460, Jul. 2004.
[9] P. E. Dyer, R. J. Farley, and R. Giedl, "Analysis and application of a order Talbot interferometer for 193 nm laser grating formation," *Opt. Commun.*, vol. 129, no. 1–2. pp. 98–108, Aug. 1996.
[10] C. M. Rollinson *et al.*, "Variations of the growth of harmonic reflections in fiber Bragg gratings fabricated using phase masks," *J. Opt. Soc. Amer. A Opt. Image Sci.*, vol. 29, no. 7. p. 1259–1268, Jul. 2012.
[11] C. M. Rollinson *et al.*, "Reflections near 1030 nm from 1540 nm fibre Bragg gratings: Evidence of a complex refractive index structure," *Opt. Commun.*, vol. 256, no. 4–6, pp. 310–318, 2005.

[12] S. A. Wade *et al.*, "Effect of phase mask alignment on fiber Bragg grating spectra at harmonics of the Bragg wavelength," *J. Opt. Soc. Amer. A*, vol. 29, no. 8. p. 1597–1605, Aug. 2012.
[13] A. Barty, K. A. Nugent, D. Paganin, and A. Roberts, "Quantitative optical phase microscopy," *Opt. Lett.*, vol. 23, no. 11, pp. 817–819, Jun. 1998.
[14] E. D. Barone-Nugent, A. Barty, and K. A. Nugent, "Quantitative phase-amplitude microscopy I: Optical microscopy," *J. Microscopy*, vol. 206, no. 3, pp. 194–203, Jun. 2002.
[15] A. Barty, K. A. Nugent, A. Roberts, and D. Paganin, "Quantitative phase tomography," *Opt. Commun.*, vol. 175, no. 4–6, pp. 329–336, Mar. 2000.
[16] N. M. Dragomir, X. M. Goh, and A. Roberts, "Three-dimensional refractive index reconstruction with quantitative phase tomography," *Microscopy Res. Techn.*, vol. 71, no. 1, pp. 5–10, Jan. 2008.
[17] X. M. Goh, N. M. Dragomir, D. N. Jamieson, and A. Roberts, "Optical tomographic reconstruction of ion beam induced refractive index changes in silica," *Appl. Phys. Lett.*, vol. 91, no. 18, p. 181102, Oct. 2007.
[18] N. M. Dragomir, A. X. M. Goh, and A. Roberts, "Three-dimensional quantitative phase imaging: Current and future perspectives," in *Proc. SPIE 3-D Multidimensional Microscopy, Image Acquisition Process. XV*, 2008, p. 686106.
[19] B. P. Kouskousis, D. J. Kitcher, S. F. Collins, and G. W. Baxter, "Numerical investigation on the effects of fabrication conditions on fiber Bragg grating spectra using the phase mask technique," *Appl. Opt.*, vol. 52, no. 14, pp. 3338–3344, May 2013.
[20] L. A. Shepp and B. F. Logan, "The Fourier reconstruction of a head section," *IEEE Trans. Nucl. Sci.*, vol. NS-21, no. 3, pp. 21–43, Jun. 1974.
[21] F. Natterer, *The Mathematics of Computerized Tomography*. Stuttgart, Germany: Wiley, 1986.
[22] S. Malcolm and C. K. Avinash, *Principles of Computerized Tomographic Imaging*. New York, NY, USA: IEEE, 1988.
[23] G. N. Ramachandran and A. V. Lakshminarayanan, "Three-dimensional reconstruction from radiographs and electron micrographs: Application of convolutions instead of Fourier transforms," *Proc. Nat. Academy Sci. USA*, vol. 68, no. 9, pp. 2236–2240, Sep. 1971.
[24] Amira. [Online]. Available: http://www.amira.com
[25] K. W. Raine, R. Feced, S. E. Kanellopoulos, and V. A. Handerek, "Measurement of axial stress at high spatial resolution in ultraviolet-exposed fibers," *Appl. Opt.*, vol. 38, no. 7, pp. 1086–1095, Mar. 1999.